Prolonged seismically induced erosion and the mass balance of a large earthquake ☆

Niels Hovius [a,*], Patrick Meunier [b], Lin Ching-Weei [c,1], Chen Hongey [d,2], Chen Yue-Gau [d,2], Simon Dadson [e,3], Horng Ming-Jame [f], Max Lines [a]

[a] Department of Earth Sciences, University of Cambridge, Downing Street, Cambridge, CB2 3EQ, UK
[b] Laboratoire de Géologie, École Normale Supérieure de Paris, CNRS UMR 8538, 24 Rue Lhomond, 75231 Paris CEDEX 5, France
[c] Department of Earth Sciences and Disaster Prevention Research Centre, National Cheng Kung University, 1 Ta-Hsueh Road, Tainan, Taiwan, ROC
[d] Department of Geosciences, National Taiwan University, No. 1, Sec. 4, Roosevelt Road, Taipei, Taiwan, ROC
[e] Centre for Ecology and Hydrology, Maclean Building, Crowmarsh Gifford, Wallingford, OX10 8BB, UK
[f] Water Resources Agency, Ministry of Economic Affairs, Hsin-Yi Road, Taipei, Taiwan, ROC

ABSTRACT

Large earthquakes deform the Earth's surface and drive topographic growth in the frontal zones of mountain belts. They also induce widespread mass wasting, reducing relief. The sum of these two opposing effects is unknown. Using a time series of landslide maps and suspended sediment transport data, we show that the M_W7.6 Chi-Chi earthquake in Taiwan was followed by a period of enhanced mass wasting and fluvial sediment evacuation, peaking at more than five times the background rate and returning progressively to pre-earthquake levels in about six years. Therefore it is now possible to calculate the mass balance and topographic effect of the earthquake. The Choshui River has removed sediment representing more than 30% of the added rock mass from the epicentral area. This has resulted in a reduction of surface uplift by up to 0.25 m, or 35% of local elevation change, and a reduction of the area where the Chi-Chi earthquake has built topography. For other large earthquakes, erosion may evolve in similar, predictable ways, reducing the efficiency of mountain building in fold-and-thrust belts and the topographic expression of seismogenic faults, prolonging the risk of triggered processes, and impeding economic regeneration of epicentral areas.

© 2011 Elsevier B.V. All rights reserved.

1. Introduction

The topography of the Earth's surface is the sum result of geological processes that create relief, and erosional and depositional processes that reduce relief. In many areas with high rates of crustal deformation, shallow earthquakes contribute importantly to the displacement of rocks and the surface (Avouac, 2007). The largest earthquakes dominate the cumulative seismic moment release in mechanical work (Hanks and Kanamori, 1979) both globally (Buffe and Perkins, 2005), and on individual faults (e.g., Jackson and McKenzie, 1999). Thus it is reasonable to expect that in seismically active areas topographic relief is formed mainly by large earthquakes.

However, in uplands with sufficiently steep relief, large earthquakes also cause slope failure and the conversion of rock mass into transportable sediment. Intense mass wasting has been reported from the epicentres of many large earthquakes (e.g., Chigira et al., 2010; Garwood et al., 1979; Harp and Jibson, 1996; Huang and Li, 2009; Keefer, 1984; Oldham, 1899; Sato et al., 2007; Simonett, 1967). Where relevant data exist, the rate of slope failure appears to be proportional to the peak ground acceleration (Meunier et al., 2007) or peak ground velocity caused by an earthquake, and a relation between earthquake moment and landslide volume, attributing a larger erosional impact to larger earthquakes, has been proposed (Keefer, 1994). If the products of seismically induced mass wasting are removed from the epicentral landscape (cf. Dadson et al., 2004; Pain and Bowler, 1973; Pearce and Watson, 1986), then erosion should be considered as a term in the mass balance of an earthquake. The potential importance of this term is perhaps best illustrated by the 47 km³ estimated volume of landslides triggered by the 1950, M8.6 Assam earthquake in the Tibet Himalayas (Mathur, 1953), and the 74–400 mm estimated average surface lowering by landslides caused by a M7.9 earthquake in the Torricelli Mountains of Papua New Guinea in 1935 (Simonett, 1967). However, these estimates are not optimally constrained, and they represent average or total erosion over large areas, rather than site-specific values that may be used to estimate the local topographic effect of an earthquake.
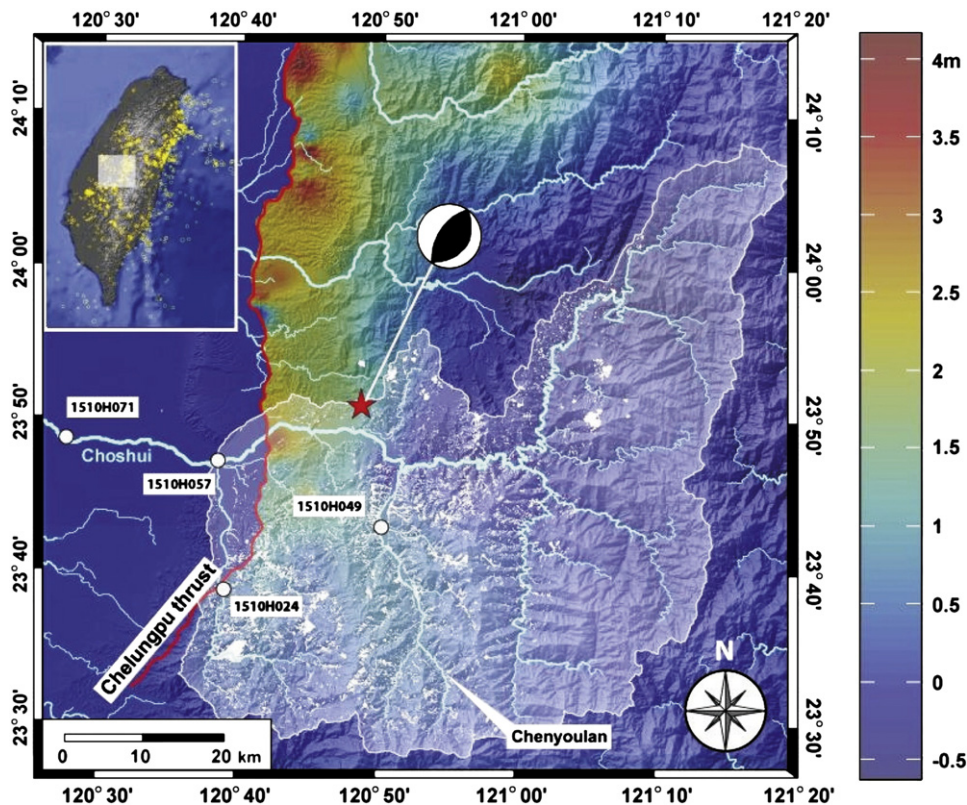
Fig. 1. Overview of the study area. Shaded relief map of the epicentral area of the Chi-Chi earthquake, showing the surface trace of the Chelungpu fault (red line), earthquake epicentre (star), surface uplift pattern (scale bar right) from Loevenbruck et al., 2004, drainage network (blue lines), co-seismic landslides (white polygons) and hydrometric stations (circles, labels give WRA station number). Masked area is the Choshui catchment (2800 km^2) within which the mass balance and net topographic effect of the earthquake have been calculated. The location of the Chenyoulan sub-catchment, where mass wasting was studied in detail, is also indicated. Inset shows the location of earthquakes with $M_W \geq 3$ from 11 September 1999 and until end of 2008 in and around Taiwan, and location of the main figure.

In the estimation of the erosional impact of an earthquake, five steps must be taken. The first is the conversion from landslide area, which can be determined from remote sensed imagery, to landslide volume. In most cases this is done using a poorly defined relation between these quantities. Although a robust global scaling law is emerging (Guzzetti et al., 2009), adjustments to local conditions will remain necessary (cf. Parise and Jibson, 2000). The second step concerns the transfer of hillslope mass wasting products into the fluvial channel system, and the subsequent export of this material. Most landslides have short trajectories, limiting their geophysical effect (Lajeunesse et al., 2005; Lin et al., 2008; Nicoletti and Sorrisovalvo, 1991). Only sediment exported from the epicentral area contributes to the net effect of an earthquake. If quantification of bulk erosion is the objective, then fluvial export is critical, and landslide volume (step 1) can be ignored. Fluvial export can be estimated from measurements of water discharge and sediment concentrations (Dadson et al., 2003; Fuller et al., 2003). The third step is the separation of erosion that would have occurred in the epicentral area if an earthquake had not happened, from erosion that is uniquely attributable to that earthquake. This requires knowledge of erosion rates and patterns prior to an earthquake (Dadson et al., 2004). The fourth step is the definition of the time period over which the erosional effect of an earthquake dissipates (cf. Koi et al., 2008; Korup, 2005; Lin et al., 2006; Ohmori, 1992). Many co-seismic landslides terminate on hillslopes and their debris can be remobilised in a mass wasting cascade at a later time (cf. Benda and Dunne, 1997; Dadson et al., 2004). Moreover, earthquake strong ground motion can enhance substrate erodibility through shattering of rock mass and coalescence of cracks (Harp and Jibson, 1996). These are lingering effects, causing enhanced erosion to persist after an earthquake (Lin

et al., 2008). A time series of landslide and fluvial sediment transport measurements is required to constrain its decay. The fifth step concerns the distribution of erosion within an earthquake epicentral area (Meunier et al., 2007). This distribution sets the local topographic effect of an earthquake for a given distribution of co-and post seismic surface deformations. It can be determined from mapped landslide patterns if hillslope mass wasting and fluvial sediment export are effectively coupled.

This pathway of quantification has never been completed for a single earthquake. As a result, the mass balance and net topographic effect of a large seismic event have never been estimated reliably. Here we do this for the $M_W 7.6$ Chi-Chi earthquake of 21 September 1999 in Taiwan, focussing initially on the fluvial export of sediment from the epicentral area, the identification of a fluvial response time, and the isolation of a seismically generated river sediment load. We then turn to the pattern of hillslope mass wasting and use it to determine the distribution of erosional surface lowering within the epicentral area. Finally, we calculate the net topographic effect, and a conservative mass balance of the Chi-Chi earthquake, and explore its implications for the mechanisms of mountain building.

2. Setting

Taiwan is the product of collision between the Luzon arc on the Philippine Sea plate and Asia. Crustal shortening at ~90 mm yr^{-1} (Sella et al., 2002) accompanied by frequent, large earthquakes, has resulted in the construction of a high mountain belt. Most recent, shallow earthquakes have occurred on north–south trending, range-bounding structures (Carena et al., 2002). In the west, these structures define a fold-and-thrust belt in the inverted Plio–Pleistocene foreland
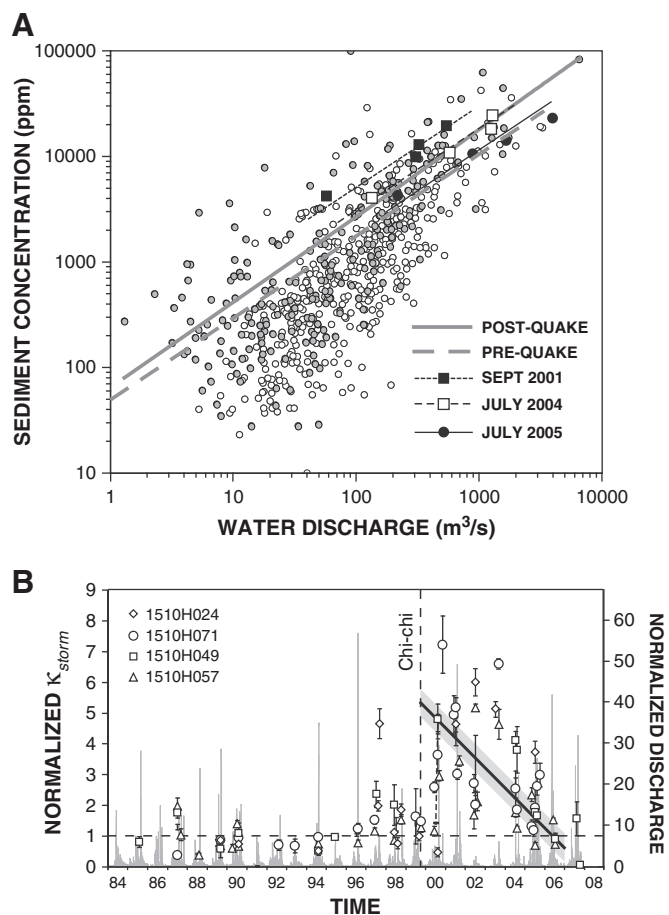
Fig. 2. Hydrometric data for the Choshui River. A) Water discharge (Q_w, m³ s⁻¹) and suspended sediment concentration (C, ppm) measured between 1987 and 2006 at the station 1510H057 on the main stream. Measurements before and after the Chi-Chi earthquake are shown as open and grey filled circles, respectively. The grey dashed line is the best-fit power law to all measurements prior to the Chi-Chi earthquake (1987–1999), of the form $C = \kappa Q_w^b$, with $b = 0.78$ and $\kappa = 47$ ppm obtained with a least-squares loss function ($R^2 = 0.45$). The solid grey line is the best power law to all post-earthquake measurements, with $b = 0.82$ and $\kappa = 59$ ppm ($R^2 = 0.55$). Filled and open squares and filled circles show data for floods in 2001, 2004, and 2005, respectively, and are subsets of the post-Chi-Chi measurement series. Data for individual floods have been fit by a power law with a fixed $b = 0.78$. B) Time evolution of the unit sediment concentration in major storm floods, κ_{storm}, at 4 stations in the Choshui catchment (error bars show 1σ range). For direct comparison, values have been normalised to the mean of values prior to September 1999 at a station. The linear least squares best fit to the post-earthquake data ($R^2 = 0.54$) shows relaxation of the unit sediment concentrations from a peak after the earthquake in 6 ± 0.8 yr (1σ shown in grey). Non-linear models do not have a significantly better fit. Water discharge, normalised to the average of 1984–2007 (~150 m³ s⁻¹), is shown in the background.

basin and older continental margin sediments. Its three principal faults, which take up an estimated 30 mm yr⁻¹ of shortening (Simoes et al., 2007) are traced by topographic ridges with up to two kilometres of relief, underlain by moderately consolidated, clastic sediments, and dissected by rivers linking the high mountains of the Central Range with the Taiwan Strait (Fig. 1). These faults merge at depth into an east-dipping detachment, on which aseismic slip is thought to occur below the Central Range (Dominguez et al., 2003).

The Chi-Chi earthquake ruptured the Chelungpu thrust fault in west Taiwan over a length of ~100 km. It had a focal depth of ~8 km, and a rupture plane dipping ~30°, merging eastward into a shallow detachment (Kao and Chen, 2000; Shin and Teng, 2001). The earthquake was the largest in Taiwan for over 60 yr, but since 2 ka five similar events have occurred on the Chelungpu fault (Streig et al., 2007). At the northern end of the rupture zone, lateral ramping has

complicated seismic surface deformation. Further south the earthquake caused up to 3 m uplift on the fault break, decreasing to zero over a distance of ~30 km to the east (Loevenbruck et al., 2004; Yu et al., 2001) (Fig. 1). Beyond, an area of subsidence extended over 50 km east of the fault.

The area affected by surface deformation during the Chi-Chi earthquake has a wet sub-tropical climate with 2–4 m of rainfall per year. Typhoons with daily rainfall rates in excess of 300 mm occur most years (Stark et al., 2010; West et al., 2011), giving rise to rapid variations in fluvial discharge of up to three orders of magnitude at a station. Typhoon precipitation drives mass wasting in Taiwan (Dadson et al., 2003), and associated floods carry the bulk of the erosion product to the ocean (Dadson et al., 2005; Hilton et al., 2008, 2011; Milliman and Kao, 2005).

The Chi-Chi earthquake has enhanced hillslope mass wasting and fluvial sediment transport during subsequent typhoons (Dadson et al., 2004; Lin et al., 2008). Sediment mobilisation on hillslopes in the epicentral area is mainly by landsliding, but sediment export is only by fluvial transport. Whilst the total effective erosion due to the earthquake can be assessed from the sediment load of rivers draining the hanging wall of the Chelungpu fault, the pattern of sediment mobilisation in this area is tied with the distribution of landslides. We have quantified both, using landslide maps obtained from SPOT and Formosat satellite images, and air photos with spatial resolutions of 12.5, 8.0, and 0.5 m, respectively (cf. Lin et al., 2003), and hydrometric data collected at gauging stations of the Taiwan Water Resources Agency (W.R.A., 1970–2008). These data comprise hourly water discharge from stage recorders, and suspended sediment concentrations measured intermittently using USDH-48 samplers. Bedload measurements are not available. Our study is limited to the epicentral Choshui River catchment, 2800 km², covering the full width of the zone affected by earthquake surface deformation (Fig. 1).

3. Fluvial sediment export

Because we do not have a robust landslide area–volume relation for the area affected by the Chi-Chi earthquake (cf. Yanites et al., 2010), and because we are primarily interested in the erosional removal of material from that area, we start our calculation of the earthquake mass budget by considering the sediment load of the Choshui River at station 1510H057, located at the mountain front. As in most rivers, the suspended sediment concentration C (ppm) is related to water discharge Q_w (m³ s⁻¹) by a power law, $C = \kappa Q_w^b$, where the exponent b is determined by the availability and mobilisation of sediment, and κ is the suspended sediment concentration at unit discharge (Fig. 2A). The least squares best fit to measurements made before the earthquake (1987–1999) has $b = 0.78$, $\kappa = 47$ ppm. The large range of measured suspended sediment concentrations at a given discharge, $R^2 = 0.45$ for the least squares best fit, reflects the natural variability of the timing, location and magnitude of sediment supply to river channels with excess transport capacity (Hovius et al., 2000). Post-earthquake data show a similar trend, but sediment concentrations were, on average, higher at all discharges, implying that the entrainment of suspendable sediment has remained efficient at the higher post-seismic supply rates. By fitting power laws to data for selected time slices, whilst keeping the exponent, b, fixed at the pre-earthquake best fit value to permit direct comparison of sediment transport, we have tracked the evolution of the unit sediment concentration κ to reveal the erosional impact of the earthquake.

Because most erosion occurs during typhoon floods (Dadson et al., 2005; Kao and Milliman, 2008), we have determined a unique κ_{storm} (cf. Milliman and Kao, 2005) for each typhoon flood with three or more suspended sediment measurements (Fig. 2A), to resolve the fluvial response to the earthquake in maximum detail. During 12 yr preceding the earthquake, κ_{storm} values at the station 1510H057 were

within a narrow range, 45 ± 6 ppm (1σ), indicating that sediment transport was tightly proportional to typhoon size (Fig. 2B). In the first significant flood after the earthquake, κ_{storm} was three times higher than the pre-earthquake average, and in July 2001, κ_{storm} topped 200 ppm (cf. Dadson et al., 2004). Since then, κ_{storm} has decreased progressively to within the pre-earthquake range of values.

To compare the history of unit sediment concentrations between four stations in the Choshui River catchment, we have normalised to the average of κ_{storm} values at each station before 1999. Unit sediment concentrations have evolved in a similar manner throughout the catchment, staying within a narrow range of values before the earthquake, peaking within two years after the earthquake, during passage of the first typhoons, and decaying since then (Fig. 2B). Although it might be expected that decay was exponential, variability in the storm data precludes confirmation. The linear least squares best fit to the combined post-earthquake data from four stations ($R^2 = 0.54$) shows normalisation of the unit sediment concentrations from a peak after the earthquake in 6 ± 0.8 yr. Non-linear models do not have a better fit.

The total excess sediment transport due to the earthquake can now be calculated as the difference between the observed transport and the background transport expected for the storm hydrograph with a specific sediment concentration fixed at the pre-earthquake mean. We have done this for the mountain front station 1510H057 where the time series of suspended sediment measurements is most complete. Fixing the unit suspended sediment concentration at $k = 45 \pm 6$ ppm, the average of storm values over the period 1987–1999, and using hourly discharge data, we estimate that typhoon floods of the Choshui River would have exported 261 Mt of suspended sediment after the earthquake and up to the end of 2007, under background conditions (Table 1). Adding 30% bed load, the average for mountain rivers in Taiwan (Dadson et al., 2003), the total fluvial export over this interval would have been 390 Mt. Bed load transport has been estimated from a comparison of bathymetrically constrained reservoir fill rates and suspended sediment transport rates in nearby catchments. Two large reservoirs, the Techi and Wushoh reservoirs, both within the area affected by the Chi-Chi earthquake, appear to have received an estimated 28% and 36% of their sediment input as bed load, respectively, averaged over the period 1970–1999. Elsewhere, bed load contributions to total river sediment load may range from 2% to 58% (Dadson et al., 2003). Others have estimated the bed load portion of the sediment load of the Lanyang River in Northeast Taiwan at 15% (Kao and Liu, 2001). Acknowledging spatial and temporal variability of bed load contributions, we have used a 30% bed load fraction in all subsequent calculations.

In reality, typhoon floods of the Choshui River after the Chi-Chi earthquake and up to the end of 2007 had a total suspended load of about 467 Mt, and an estimated total sediment load of 630 Mt (Table 1). Removing background suspended sediment load, the cumulative excess suspended sediment transport from the Choshui River catchment in typhoon floods with three or more sediment measurements in the period 2000–2007 was 206 ± 50 Mt (Table 1). To estimate excess suspended sediment transport at other times in
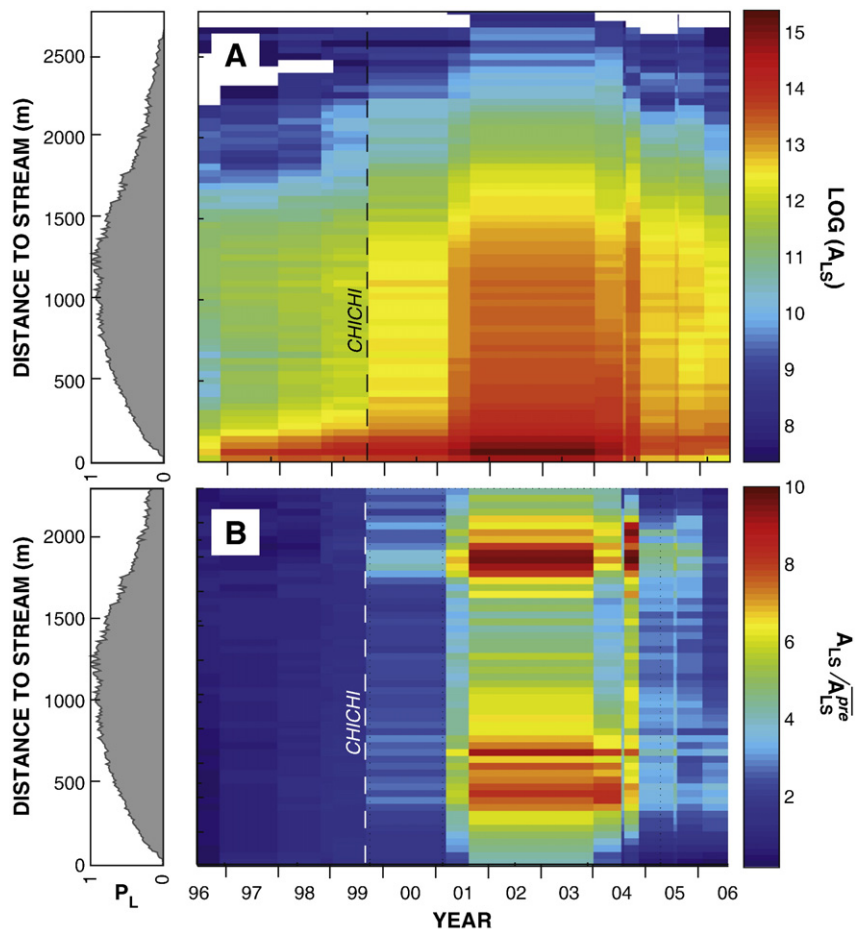
Fig. 3. Landsliding in the Chenyoulan catchment. A) Time evolution of the area of landsliding A_{LS} (m^2) reported with flow distance to stream for the period 1996–2006. The stream network is the ensemble of locations with upslope area >1 km^2. 15 time intervals are delimited by landslide maps, the difference of which represents landsliding within the interval. B) Time evolution of the area of landsliding normalised by the area of landsliding prior to the Chi-Chi earthquake (dimensionless) reported with flow distance to stream.

Table 1

Suspended sediment transport by the Choshui River at the WRA station 1510H057 in typhoon floods in 1996–2007. Magnitude of floods is indicated by total and peak discharges. Suspended sediment loads, Q_s, were calculated from flood hydrographs using $C = \kappa Q_w^b$, where C is the suspended sediment concentration, Q_w is the measured water discharge, $b = 0.7812$, and κ is the unit suspended sediment concentration. To estimate the amount of sediment that would have been carried by a flood had the Chi-Chi earthquake not occurred ($Q_{s(pre)}$), κ was fixed at the pre-earthquake mean, $\kappa = 47.12$ ppm. The actual suspended sediment load ($Q_{s(post)}$) was estimated using a κ value according to the linear least squares best fit to available flood data. The excess suspended sediment transport caused by the Chi-Chi earthquake is calculated as the difference between the two.

Typhoon	Date	Days	Total discharge (km^3)	Peak discharge (m^3/s)	κ_{storm} (ppm)	$Q_{s(pre)}$ tot (Mt)	$Q_{s(post)}$ tot (Mt)	Excess Q_s (Mt)	$\pm \sigma$ (Mt)
Herb	01/08/'96	31	2.13	8860	32.8	57			
Bilis	23/08/'00	31	1.47	4610	198	21.5	70.5	49	22
Toraji	30/07/'01	31	1.73	7660	133	41	120	79	10
Nari	17/09/'01	31	1.19	2070	133	10.5	29.5	19	5
Mindulle	02/07/'04	31	1.40	3152	79	21.5	39	17.5	3.5
Aere	24/08/'04	31	1.35	1590	57	16	28	12	2.2
Tropical Storm	13/05/'05	10	0.40	1552	91	3.5	5.5	2	0.2
Haitang	18/07/'05	17	1.16	3973	37	22.5	31.5	9	4.8
Matsa	05/08/'05	9	1.22	4083	70	26.5	37	10.5	1
Huaning	13/08/'05	19	0.66	1760	24	5	7	2	0.5
Isang	01/09/'05	31	0.95	2673	30	9	12	3	0.4
Tropical Storm	09/06/'06	10	1.68	4930	34	42.5	45.5	3	0.2
Sepat	18/08/'07	31	2.75	4091	74	42	42	0	0
				Total typhoon (Mt)		261.5	467.5	206	49.80
				Total transport (Mt)		390	630	240	60
				Volume (km^3)		0.14	0.23	0.1	0.015
				Erosion (mm)		52	84	32	5

this interval, we have used $C = \kappa Q_w^b$, with κ evolving as the best fit to κ_{storm} estimates, and hourly discharges at the station. The excess suspended load of these discharges was 34 ± 10 Mt, bringing the total excess suspended sediment load of the Choshui River up to the end of 2007, and over the full decay time to 240 ± 60 Mt. Adding 30% bed load, we estimate that the Choshui River has exported 320 ± 80 Mt seismically produced sediment from the hanging wall of the Chelungpu fault since the Chi-Chi earthquake, in addition to a total of 520 ± 20 Mt of sediment that would have been removed had the earthquake not occurred. The excess sediment load represents the erosional effect of the Chi-Chi earthquake within the Choshui catchment. This estimate is conservative. The best free fit to all pre-earthquake storm data at the station 1510H057 has $\kappa = 66 \pm 13$ and $b = 0.72$. Use of these values would reduce the estimate of excess suspended sediment transport by only 5 Mt. Free fits to data for individual storms would add 40 Mt to the excess transport estimate.

4. Mass wasting and sediment supply

Next, we determine the supply mechanism of the river sediment, focussing on the Chenyoulan Chi tributary, 367 km^2 (Fig. 1), which joins the Choshui main stream 12 km south of the earthquake epicentre. In this catchment, the history of mass wasting is known in unique detail from 16 landslide maps covering 1996–2006. 8123 mapped landslides with a combined surface area of 31.5 km^2 occurred prior to the Chi-Chi earthquake. 3800 mapped landslides with a combined area of 16 km^2 have been attributed to the earthquake, and 48,370 landslides with a total area of 221 km^2 have occurred after the earthquake and up to the end of 2006. These landslides were triggered by intense, but unexceptional typhoon rainfall. They were largely unrelated to aftershocks whose summed moment normalised within 15 months after the Chi-Chi earthquake (Hsu et al., 2009).

The density and position of landslides with respect to slope-bounding streams in the Chenyoulan catchment are shown in Fig. 3A. Prior to 1999, landslides primarily occurred on slope segments adjacent to river channels. Rates of landsliding increased throughout the landscape due to the earthquake (Fig. 3B), with maximum changes of up to 800% at 300–700 m from streams, and also at 1700–2200 m from streams, where many of the principal ridges are located. We attribute these changes to the weakening of rock mass due to strong ground motion, and the focussing of seismic waves in mountain ridges and other convex topography within the catchment (Meunier et al., 2008). Landslide rates have decayed steadily from a maximum in 2001, when the Chenyoulan catchment was first hit by a large typhoon (Toraji, Saffir–Simpson category 3) after the earthquake. Moreover, landsliding has migrated to lower positions on
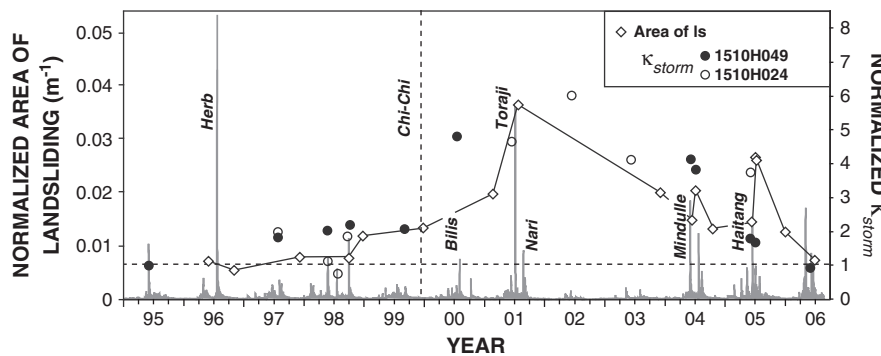

Fig. 4. Time evolution of landslide area and unit suspended sediment concentration in storm floods in the Chenyoulan catchment. The area (m^2) of landslides in a given time interval has been divided by the total water discharge (m^3) at the station 1510H049 over that interval, to normalise for strength of storm forcing of slope failure, and is shown by a data point placed at the end of the interval. κ_{storm} values have been normalised to the best fit value to all data for the station prior to September 1999. The horizontal dashed line is the average of normalised landslide areas before the Chi-Chi earthquake. Shown in the background is the hydrograph of station 1510H049, where peak height is proportional to discharge. Missing discharge data for a period in 2001–02 has been substituted with data from the stations 1510H057 and 071, scaled to account for catchment size.

hillslopes over this interval. In 2006, landslide rates on lower slopes had normalised, but they have remained somewhat elevated on higher slopes (Fig. 3B).

Landsliding and fluvial transport of suspended sediment have co-evolved in the Chi-Chi epicentral area. This is clear from a comparison of landslide densities and unit suspended sediment concentrations in the Chenyoulan River at station 1510H049 (supplemented with data from the nearby station 1510H024 for a period in 2001–02 when the station 1510H049 was broken) (Fig. 4). To normalise for strength of storm forcing of slope failure, the area (units: m^2) of landslides in a given time interval has been divided by the total water discharge (units: m^3) at the station over that interval, and this value (unit: m^{-1}) is paired with the κ value of the biggest flood in the interval. The correlation between these values is strongest for landslides within 240 m from river channels, $R^2 = 0.68$, and decreases gradually when landslides on higher slope segments are included (Fig. 5). Normalisation of landslide densities by peak storm discharge during an interval gives similar results. These findings imply that landslides are the principal source of sediment in the rivers draining the epicentral area, and that the rivers respond on timescales shorter than the time between typhoons to supply suspendable material from hillslopes. Thus, the time evolution of the suspended sediment load of rivers draining the Chi-Chi epicentral area, as shown in Fig. 2, is likely to be controlled by the time evolution of mass wasting on their interfluves. The coupling between hillslopes and river channels in this catchment is most efficient at a horizontal length scale of ~0.25 km. Landslides higher on hillslopes have not systematically delivered sediment to river channels.

The pattern of landslide density can now be used to distribute the total excess fluvial erosion over the epicentral area and to determine the net topographic effect of the Chi-Chi earthquake.

5. Mass balance and topographic effect of the Chi-Chi earthquake

We have plotted the density of landslides triggered by the earthquake in a 50 km wide corridor perpendicular to the Chelungpu fault trace, including the Choshui catchment, treating the earthquake as a linear source of energy (Fig. 6). The landslide density peaked at 3.7% in the earthquake epicentre where peak ground acceleration and

velocity were highest, and decayed exponentially to background values at ~50 km east of the fault break, closely tracking the geometric spreading and attenuation of seismic waves and ground motion (Meunier et al., 2007). Over this distance the distribution of landslides on hillslopes remained approximately constant (Fig. 7), implying that the coupling of hillslopes and river channels was uniform. Landslides triggered by subsequent typhoons had similar distributions, but different peak densities. For example during typhoon Toraji landslide density peaked at 6.6% in the earthquake epicentre, and reached background values at ~50 km from the fault break, with a secondary maximum where precipitation rates were highest (Fig. 6). In the absence of a full time series of regional landslide maps, we have used the density distribution of co-seismic landslides as a proxy for the distribution of subsequent sediment production.

Extrapolating available geodetic data (Loevenbruck et al., 2004; Yu et al., 2001), and using a rock density $\rho_r = 2.75 \times 10^3$ kg m^{-3}, we estimate that the surface deformation caused by the Chi-Chi earthquake, including afterslip, represented an addition of about 1000 Mt of rock mass to the Choshui catchment, raising its surface by an average of 13 cm. The maximum average surface uplift was 1.3 m, on the Chelungpu fault, decreasing to zero at 30 km east of the fault break. Beyond, the hanging wall subsided (Figs. 1 and 6). The earthquake also caused erosion of 320 ± 80 Mt of sediment from this catchment, reducing added surface elevation by 4.3 ± 0.7 cm, or $32 \pm 8\%$ on average. Assuming that seismically induced erosion was distributed according to the pattern of co-seismic landslide density, erosion peaked at 13 ± 2 cm in the earthquake epicentre (23 ± 4 cm when using the greater landslide density associated with typhoon Toraji), caused a reduction of the area over which the earthquake resulted in net topographic growth, and added to co-seismic subsidence in the distant hanging wall (Fig. 6). When background erosion is taken into account, 840 ± 100 Mt of sediment may have been removed from the Choshui catchment since the earthquake and up to the end of 2007. This represents an average surface lowering of
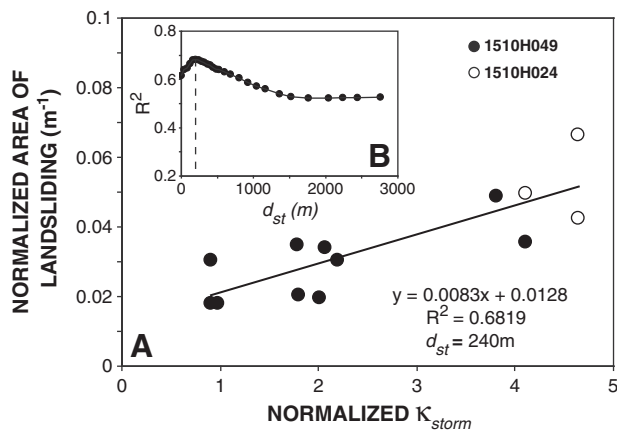
Fig. 5. A) Correlation of landslide area in the Chenyoulan catchment and the unit suspended sediment concentration in storm floods (normalised as in Fig. 2) at the catchment outlet station 1510H049. For a period in 2001 -02, when this station was broken, data from the nearby station 1510H024, located outside the Chenyoulan catchment, have been used instead. The area (m^2) of landslides in a given time interval has been divided by the total water discharge (m^3) at the station over that interval, to normalise for strength of storm forcing of slope failure. This value is paired with the κ value of the biggest flood in the interval, and the black line is the linear best fit. The best correlation, $R^2 = 0.68$, is found for landslide density measured within 240 m from streams (d_{st}). B) Strength of correlation, R^2, of normalised landslide area within distance d_{st} from stream with κ_{storm}.
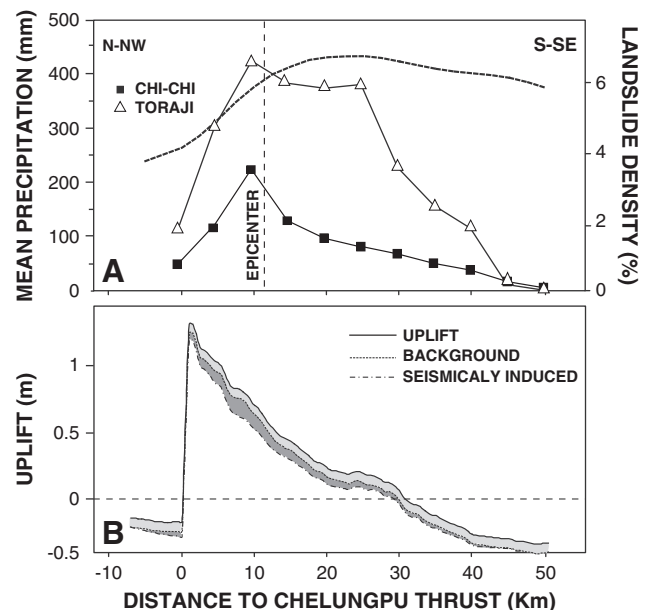
Fig. 6. Distribution of uplift and erosion caused by Chi-Chi earthquake. A) Density of landslides triggered by the earthquake and Toraji, 2001, the first major typhoon to hit the epicentral area, plotted with distance to the surface trace of the Chelungpu fault. The density distribution of typhoon-triggered landslides follows the same general pattern as the co-seismic landslides, but also reflects the spatial pattern of rainfall intensity shown by bold black line. B) Topographic effect of the Chi-Chi earthquake through the Choshui catchment. The Seismic uplift of catchment surface (black) has been reduced by background erosion (light grey), assumed to be uniformly distributed, and additional erosion caused by the earthquake (dark grey), distributed according to density of co-seismic landslides.
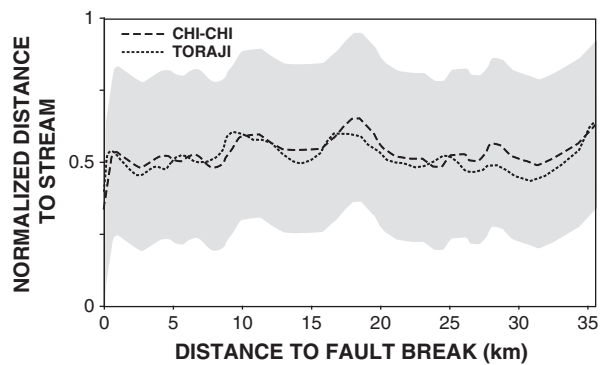
Fig. 7. Mean position of co-seismic (dashed line) and post-seismic landslides (dotted line) on slopes, and spread (1σ) of co-seismic landslides (grey area), plotted with distance to the Chenlungpu fault break. Distance to stream has been normalised to the total length of the slope (ridge crest–stream), and the stream network has been defined as all points in the landscape with upslope area >1.0 km² (cf. Lin et al., 2008). Allowing for local variations, the position of landslides in the landscape is independent of distance to the fault break.

11 cm in the catchment and a removal of 4/5 of the rock mass added by the earthquake.

These figures include the effects of hanging wall subsidence in the Choshui headwaters. Within 30 km from the Chelungpu fault, excess and total erosion have reduced the topographic effect of the earthquake by about 16% and 34%, respectively. In the decade before the earthquake, the average catchment erosion rate was 5.3 ± 1 mm yr^{-1}, similar to the background erosion rate of 8.7 ± 1.6 mm yr^{-1} during 1999–2007. At this rate, the remaining seismically added rock mass will be removed from the Choshui catchment in 4 yr. Even the maximum average surface uplift near the fault break would be annulled well within the return time of $M_W \geq 7$ earthquakes on the Chelungpu fault.

6. Discussion and conclusions

The Chi-Chi earthquake has caused relatively little displacement on the southern segment of the Chelungpu fault, intersecting the Choshui River catchment. Horizontal slip increased northward to 10–15 m (Ji et al., 2001) and uplift reached up to 3 m, augmented about 10% by afterslip (Hsu et al., 2009), with local extremes of 8 m (Chen et al., 2001). With return times of ~400 yr for historic large earthquakes on the Chelungpu fault (Streig et al., 2007), and historic erosion rates of ~5 mm yr^{-1} (theromochronometric constrains on long term erosion rates are not available), such offsets could equal or exceed seismically-induced and interseismic erosion, and result in mountain building. However, where crustal shortening is accommodated on a shallow detachment, mainly by slip in large earthquakes, as in the western foothills of Taiwan, average surface elevation is significantly reduced by erosion caused by the same mechanism that constructs topography. This subdues the surface taper of frontal ranges, and could hamper the recognition of active, seismogenic faults (e.g., Wobus et al., 2005). Notably, the seismogenic potential of the Chelungpu fault has long been underrated as a result of its subdued topographic expression (Chen et al., 2002) (Fig. 1), with less than 200 m of relief across the fault in many places. Inside the mountain belt, where the detachment is deeper, slip is largely aseismic (Dominguez et al., 2003) with less attendant erosion, and therefore more effective in mountain building.

From a geophysical perspective it is, ultimately, the export of sediment from an epicentral area that is important in the mass balance of an earthquake. Most sediment produced by large earthquakes is mobilised by landslides, many of which stop on hillslopes and do not deliver sediment to river channels. Although this material is eventually eroded from the landscape in settings where persistent tectonic forcing maintains a lasting downslope cascade of sediment, its removal is convolved with the transfer of sediment liberated by a-seismic processes. Our analysis suggests that it may be difficult to isolate this long-term, seismically induced erosion flux from the ambient sediment load of rivers. It is, therefore, likely that the total erosional effect of the Chi-Chi earthquake is significantly larger than our estimate from resolvable excess river suspended loads, reducing further its net contribution to mountain building in west Taiwan. Only the isolation of a seismically sourced sediment flux in the background fluvial sediment load would permit true closure of the earthquake mass balance calculation.

One way of achieving this would be through a complete census of earthquake-induced landslides, assuming that their debris will eventually be evacuated from the catchment. Independent estimates of the volume of seismically induced landslides within the 0.2 g contour of the Chi-Chi earthquake, using previously published landslide data (Dadson et al., 2004) and a landslide area–volume scaling relation calibrated with observations from New Zealand (Hovius et al., 1997), are in the range of $0.5–1.3 \times 10^4$ Mt (Yanites et al., 2010). Complete removal of landslide material, according to these estimates, would give an average landscape lowering of 0.6–1.7 m (Yanites et al., 2010), several times larger than the average surface uplift induced by the Chi-Chi earthquake in its epicentral area. If correct, this would pose profound questions about the nature of mountain building. However, it is not clear that landslide area–volume relations from New Zealand apply in Taiwan, and landslides may well have been shallower than implied in the calculations, certainly where locations have suffered repeated landsliding after the earthquake (Lin et al., 2008). Importantly, landslide area–volume relations are for source areas only. Because most Taiwanese landslide data does not permit separation of source and deposit, use of affected area would give rise to a substantial overestimation of mobilised volumes. In addition, much of the landslide debris may still be in the epicentral landscape (Fig. 3). The time scale of its removal is unknown, but it is possible that seismically induced landslide debris deposited on hillslopes could take on average more than one seismic cycle to reach the fluvial channel network. Once there, coarse landslide debris (cf. Attal and Lavé, 2006) may take decades to centuries to travel downstream as bed load (Yanites et al., 2010), causing long-lived and substantial aggradation of river channels (Chen and Petley, 2005; Hsu et al., 2010). If the fluvial transport capacity allowed this, then the surplus of bed load material in the channel network could also result in elevated bed load contributions to the total river sediment load. However, bedrock channel alluviation is a general phenomenon in Taiwan (Turowski et al., 2008), and unlikely to have a unique effect on bed load contributions in the Chi-Chi epicentral area. On balance, we do not see strong evidence for the erosional effect of the Chi-Chi earthquake comprehensively outstripping seismic surface deformation.

Preliminary work elsewhere (Parker, 2010; A. Densmore, pers. comm. 2010) indicates that some large earthquakes may indeed have a negative mass balance due to the pairing of limited surface deformation with very high rates of seismically induced mass wasting. This could be most likely for earthquakes with a large strike–slip component, such as the 2008 M_w 7.9 Wenchuan earthquake (Huang and Li, 2009; Hubbard and Shaw, 2009). However, available figures for the 1950, M_w 8.6 Assam earthquake suggest that this shallow thrust event (Chen and Molnar, 1977) in the eastern Himalayan syntaxis may also have had a net mass budget strongly reduced by seismically induced erosion. If the earthquake did indeed cause landslides with a total volume of 47 km³ as reported by Mathur (1953), then this is equivalent to erosional surface lowering of about 2 m averaged over the extent of the 250 km long and 100 km wide rupture zone (Molnar and Pandey, 1989), presumably with much higher values in the smaller areas with strongest ground motion and greatest surface uplift.

The association of co-seismic landsliding and earthquake strong ground motion is universal. This may give rise to a characteristic and predictable erosion pattern during large earthquakes (Meunier et al., 2007, 2008), the amplitude of which may vary significantly between earthquakes (Keefer, 1994). In the Chi-Chi epicentral area this pattern is long-lived, and the seismically agitated landscape has remained primed for erosion during subsequent trigger events. The eradication of this weakness has taken about six years in the case of the Chi-Chi earthquake, but this time constraint cannot be exported indiscriminately due to differences in earthquake mechanism, substrate and climate. Instead the depth of erosion may be used to assess the degree of relaxation. In our example, an average of 7.5 cm of rock mass had been removed from the area affected by seismically induced landsliding, bounded by the 0.1 g contour of vertical peak ground acceleration, when erosion normalised. This was the cumulative effect of ten tropical cyclones ranging in size up to Saffir–Simpson category 3, and a number of lesser storms, which together triggered about 10 times more landslides than the Chi-Chi earthquake itself. Thus, the erosional effect of large earthquakes endures in landscapes with large topographic relief, whilst the normalisation of erosion rates in an epicentral area can be quantified, and may be predicted for the benefit of improved management of ongoing and future earthquake disasters and ensuing economic regeneration.

Acknowledgments

References

Attal, M., Lavé, J., 2006. Changes of bedload characteristics along the Marsyandi River (central Nepal): implications for understanding hillslope sediment supply, sediment load evolution along fluvial networks, and denudation in active orogenic belts. In: Willett, S.D., et al. (Ed.), Tectonics, Climate, and Landscape Evolution: Geological Society of America Special Paper 398, pp. 143–171.

Avouac, J.P., 2007. Dynamic processes in extensional and expressional settings — mountain building: from earthquakes to geological deformation. Treatise Geophys. 6, 37–439.

Benda, L., Dunne, T., 1997. Stochastic forcing of sediment supply to channel networks from landsliding and debris flow. Water Resour. Res. 33, 2849–2863.

Buffe, G.C., Perkins, D.M., 2005. Evidence for a global seismic-moment release sequence. Bull. Seismol. Soc. Am. 95, 833–853.

Carena, S., Suppe, J., Kao, H., 2002. Active detachment of Taiwan illuminated by small earthquakes and its control of first-order topography. Geology 30, 935–938.

Chen, W.P., Molnar, P., 1977. Seismic moments of major earthquakes and the average rate of slip in central Asia. J. Geophys. Res. 82, 2945–2969.

Chen, H., Petley, D.N., 2005. The impact of landslides and debris flows triggered by typhoon Mindulle in Taiwan. Q. J. Eng. Geol. Hydrogeol. 38, 301–304.

Chen, Y.G., Chen, W.S., Lee, J.C., Lee, Y.H., Lee, C.T., Chang, H.C., Lo, C.H., 2001. Surface rupture of 1999 Chi-Chi earthquake yields insights on active tectonics of central Taiwan: seism. Soc. Am. Bull. 91, 977–985.

Chen, Y.G., Chen, W.S., Wang, Y., Lo, P.W., Liu, T.K., Lee, J.C., 2002. Geomorphic evidence for prior earthquakes: lessons from the 1999 Chichi earthquake in central Taiwan. Geology 30, 171–174.

Chigira, M., Wu, X., Inokuchi, T., Wang, G., 2010. Landslides induced by the 2008 Wenchuan earthquake, Sichuan, China. Geomorphology 118, 225–238.

Dadson, S.J., Hovius, N., Chen, H., Dade, W.B., Hsieh, M.L., Willett, S.D., Hu, J.C., Horng, M.J., Chen, M.C., Stark, C.P., Lague, D., Lin, J.C., 2003. Links between erosion, runoff variability and seismicity in the Taiwan orogen. Nature 426, 648–651.

Dadson, S.J., Hovius, N., Chen, H., Dade, W.B., Lin, J.C., Hsu, M.L., Lin, C.W., Horng, M.J., Tien, T.C., Milliman, J., Stark, C.P., 2004. Earthquake-triggered increase in sediment delivery from an active mountain belt. Geology 32, 733–736.

Dadson, S.J., Hovius, N., Pegg, S., Dade, W.B., Horng, M.J., Chen, H., 2005. Hyperpycnal river flows from an active mountain belt. J. Geophys. Res. 110, F04016. doi:10.1029/2004JF000244.

Dominguez, S., Avouac, J.-P., Michel, R., 2003. Horizontal coseismic deformation of the 1999 Chi-Chi earthquake measured from SPOT satellite images: implications for the seismic cycle along the western foothills of central Taiwan. J. Geophys. Res. 108. doi:10.1029/2001JB000951.

Fuller, C.W., Willett, S.D., Hovius, N., Slingerland, R., 2003. Erosion rates for Taiwan mountain basins: New determinations from suspended sediment records and a stochastic model of their temporal variation. J. Geol. 111, 71–87.

Garwood, N.C., Janos, D.P., Brokaw, N., 1979. Earthquake-caused landslides: a major disturbance to tropical forests. Science 205, 997–999.

Guzzetti, F., Ardizzone, F., Cardinali, M., Rossi, M., Valiga, D., 2009. Landslide volumes and landslide mobilization rates in Umbria, Central Italy. Earth Planet. Sci. Lett. 279, 222–229.

Hanks, T.C., Kanamori, H., 1979. Moment magnitude scale. J. Geophys. Res. 84, 2348–2350.

Harp, E.L., Jibson, R.W., 1996. Landslides triggered by the 1994 Northridge, California, earthquake. Bull. Seismol. Soc. Am. 86, 319–332.

Hilton, R.G., Galy, A., Hovius, N., Chen, M.C., Horng, M.J., Chen, H., 2008. Tropical cyclones drive erosion of terrestrial organic carbon from mountain slopes to the deep ocean. Nat. Geosci. 1, 759–762.

Hilton, R.G., Galy, A., Hovius, N., Horng, M.J., Chen, H., 2011. Efficient transport of fossil organic carbon to the ocean by steep mountain rivers: an organic carbon sequestration mechanism. Geology 39, 71–74.

Hovius, N., Stark, C.P., Allen, P.A., 1997. Sediment flux from a mountain belt derived by landslide mapping. Geology 25, 231–234.

Hovius, N., Stark, C.P., Chu, H.-T., Lin, J.-C., 2000. Supply and removal of sediment in a landslide-dominated mountain belt: Central Range, Taiwan. J. Geol. 108, 73–89.

Hsu, Y.J., Avouac, J.P., Yu, S.B., Chang, C.H., Wu, Y.M., Woessner, J., 2009. Spatio-temporal slip, and stress level on the faults within the western foothills of Taiwan: implications for fault frictional properties. Pure Appl. Geophys. 166, 1853–1884.

Hsu, H.L., Yanites, B.J., Chen, C.C., Chen, Y.G., 2010. Bedrock detection using 2D electrical resistivity imaging along the Peikang River, central Taiwan. Geomorphology 114, 406–414.

Huang, R.Q., Li, W.L., 2009. Analysis of the geo-hazards triggered by the 12 May 2008 Wenchuan Earthquake, China. Bull. Eng. Geol. Environ. 68, 363–371.

Hubbard, J., Shaw, J.H., 2009. Uplift of the Longmen Shan and Tibetan plateau, and the 2008 Wenchuan (M = 7.9) earthquake. Nature 458, 194–197.

Jackson, J., McKenzie, D., 1999. A hectare of fresh striations on the Arkitsa fault, central Greece. J. Struct. Geol. 21, 1–6.

Ji, C., Helmberger, D.V., Song, T.R.A., Ma, K.F., Wald, D.J., 2001. Slip distribution and tectonic implications of the 1999 Chi-Chi, Taiwan earthquake. Geophys. Res. Lett. 28, 4379–4382.

Kao, H., Chen, W.P., 2000. The Chi-Chi earthquake sequence: active, out-of-sequence thrust faulting in Taiwan. Science 288, 2346–2349.

Kao, S.J., Liu, K.K., 2001. Estimating the suspended sediment load by using the historical hydrometric record from the Lanyang-Hsi watershed. Terrestr. Atm. Ocean. Sci. 12, 401–414.

Kao, S.J., Milliman, J.D., 2008. Water and sediment discharge from small mountainous rivers, Taiwan: the roles of lithology, episodic events, and human activities. J. Geol. 116, 431–448.

Keefer, D.K., 1984. Landslides caused by earthquakes. Geol. Soc. Am. Bull. 95, 406–421.

Keefer, D.K., 1994. The importance of earthquake-induced landslides to long-term slope erosion and slope-failure hazards in seismically active regions. Geomorphology 10, 265–284.

Koi, T., Hotta, N., Ishigaka, I., Matuzaki, N., Uchiyama, Y., Suzuki, M., 2008. Prolonged impact of earthquake-induced landslides on sediment yield in a mountain watershed: the Tanzawa region, Japan. Geomorphology 101, 692–702.

Korup, O., 2005. Large landslides and their effect on sediment flux in South Westland, New Zealand. Earth Surf. Process. Land. 30, 305–323.

Lajeunesse, E., Monnier, J.B., Homsy, G.M., 2005. Granular slumping on a horizontal surface. Phys. Fluids 17, 103302.

Lin, C.W., Shieh, C.L., Yuan, B.D., Shieh, Y.C., Liu, S.H., Lee, S.Y., 2003. Impact of Chi-Chi earthquake on the occurrence of landslides and debris flow: example from the Chenyulan river watershed. Eng. Geol. 71, 49–61.

Lin, W., Lin, C., Chou, W., 2006. Assessment of vegetation recovery and soil erosion at landslides caused by a catastrophic earthquake. Ecol. Eng. 28, 79–89.

Lin, G.W., Chen, H., Hovius, N., Horng, M.J., Dadson, S., Meunier, P., Lines, M., 2008. Effects of earthquake and cyclone sequencing on landsliding and fluvial sediment transfer in a mountain catchment. Earth Surf. Process. Land. 33, 1354–1373.

Loevenbruck, A., Cattin, R., Le Pichon, X., Dominguez, S., Michel, R., 2004. Coseismic slip resolution and post-seismic relaxation time of the 1999 Chi-Chi, Taiwan, earthquake as constrained by geological observations, geodetic measurements and seismicity. Geophys. J. Int. 158, 310–326.

Mathur, L.P., 1953. Assam earthquake of 15th August 1950 — a short note on factual observations. In: Ramachandra Rao, M.B. (Ed.), A Compilation of Papers on the Assam Earthquake of August 15, 1950. : The Central Board of Geophys. Publ. 1. National Geographical Research Institute, Hyderabad, India, pp. 56–60.

Meunier, P., Hovius, N., Haines, A.J., 2007. Regional patterns of earthquake-triggered landslides and their relation to ground motion. Geophys. Res. Lett. 34, L20408.

Meunier, P., Hovius, N., Haines, A.J., 2008. Topographic site effects and the location of earthquake induced landslides. Earth Planet. Sci. Lett. 275, 221–232.

Milliman, J.D., Kao, S.J., 2005. Hyperpycnal discharge of fluvial sediment to the ocean: impact of super-typhoon Herb (1996) on Taiwanese rivers. J. Geol. 113, 503–516.

Molnar, P., Pandey, M.R., 1989. Rupture zones of great earthquakes in the Himalayan region. Proc. Indian Acad. Sci. Earth Planet. Sci. 98, 61–70.

Nicoletti, P.G., Sorrisovalvo, M., 1991. Geomorphic controls of the shape and mobility of rock avalanches. Geol. Soc. Am. Bull. 103, 1365–1373.

Ohmori, H., 1992. Dynamics and erosion rate of the river running on a thick deposit supplied by a large landslide. Z. Geomorphol. 36, 129–140.

Oldham, R.D., 1899. Report on the Great Earthquake of 12 June 1897: Geological Survey of India Memoir 29.

Pain, C.F., Bowler, J.M., 1973. Denudation following the 1970 earthquake at Madang, Papua New Guinea. Z. Geomorphol. 18, 92–104.

Parise, M., Jibson, R.W., 2000. A seismic landslide susceptibility rating of geologic units based on analysis of characteristics of landslides triggered by the 17 January, 1994 Northridge, California earthquake. Eng. Geol. 58, 251–270.

Parker, R.N., 2010. Controls on the distribution of landslides triggered by the 2008 Wenchuan earthquake, Sichuan Province, China. MSCR thesis 60280, University of Durham, 225 pp.

Pearce, A.J., Watson, A.J., 1986. Effects of earthquake-induced landslides on sediment budget and transport over 50 years. Geology 14, 52–55.

Sato, H.P., Hasegawa, H., Fujiwara, S., Tobita, M., Koarai, M., Une, H., Iwahashi, J., 2007. Interpretation of landslide distribution triggered by the 2005 Northern Pakistan earthquake using SPOT 5 imagery. Landslides 4, 113–122.

Sella, G.F., Dixon, T.H., Mao, A., 2002. REVEL: a model for recent plate velocities from space geodesy. J. Geophys. Res. 107, 2081. doi:10.1029/2000JB000033.

Shin, T.C., Teng, T.L., 2001. An overview of the 1999 Chi-Chi, Taiwan, earthquake. Bull. Seismol. Soc. Am. 91, 895–913.

Simoes, M., Avouac, J.P., Chen, Y.G., 2007. Slip rates on the Chelungpu and Chushiang thrust faults inferred from a deformed strath terrace along the Dungpuna river, West Central Taiwan. J. Geophys. Res. 112. doi:10.1029/2005JB004200.

Simonett, D.S., 1967. Landslide distribution and earthquakes in the Bewani and Torricelli Mountains, New Guinea — a statistical analysis. In: Jennings, J.N., Mabbutt, J.A. (Eds.), Landform Studies from Australia and New Guinea. Cambridge University Press, Cambridge, pp. 64–84.

Stark, C.P., Barbour, J.R., Hayakawa, Y.S., Hattanji, T., Hovius, N., Chen, H., Lin, C.-W., Horng, M.-J., Xu, K.Q., Fukahata, Y., 2010. The climatic signature of incised river meanders. Science 327, 1497–1501.

Streig, A.R., Rubin, C.M., Chen, W.S., Chen, Y.G., Lee, L.S., Thompson, S.C., Madden, C., Lu, S.T., 2007. Evidence for prehistoric coseismic folding along the Tsaotun segment of the Chelungpu fault near Nan-Tou, Taiwan. J. Geophys. Res. 112. doi:10.1029/2006JB004493.

Turowski, J.M., Hovius, N., Wilson, A., Horng, M.J., 2008. Hydraulic geometry, river sediment and the definition of bedrock channels. Geomorphology 99, 26–38.

Water Resources Agency, 1970–2008. Hydrological Yearbook of Taiwan, Republic of China: Taipei; also available at http://gweb.wra.gov.tw/wrweb.

West, A.J., Lin, C.W., Lin, T.C., Hilton, R.G., Tanaka, M., Chang, C.T., Lin, K.C., Galy, A., Sparkes, R., Hovius, N., 2011. Mobilization and transport of coarse woody debris by large storms. Limnol. Oceanogr. 56, 77–85.

Wobus, C., Heimsath, A., Whipple, K., Hodges, K., 2005. Active out-of-sequence thrust faulting in the central Nepalese Himalaya. Nature 434, 1008–1011.

Yanites, B.J., Tucker, G.E., Mueller, K.J., Chen, Y.G., 2010. How rivers react to large earthquakes: evidence from central Taiwan. Geology 38, 639–642.

Yu, S.B., Kuo, L.C., Hsu, Y.J., Su, H.H., Liu, C.C., Hou, C.S., Lee, J.F., Lai, T.C., Liu, C.C., Liu, C.L., Tseng, T.F., Tsai, T.S., Shin, T.C., 2001. Preseismic deformation and coseismic displacements associated with the 1999 Chi-Chi, Taiwan, earthquake. Bull. Seismol. Soc. Am. 91, 995–1012.